Biosynthesis of magnesium oxide (MgO) nanoflakes by using leaf extract of Bauhinia purpurea and evaluation of its antibacterial property against Staphylococcus aureus

Article *in* Materials Science and Engineering C · May 2018

DOI: 10.1016/j.msec.2018.05.059

CITATIONS
90

READS
1,422

9 authors, including:

Bhaskar Das
National Institute of Technology Rourkela
34 PUBLICATIONS **1,222** CITATIONS
SEE PROFILE

Moumita Sahoo
National Innovation Foundation- India
16 PUBLICATIONS **301** CITATIONS
SEE PROFILE

Soumen Ghosh
KIIT University
3 PUBLICATIONS **160** CITATIONS
SEE PROFILE

Md. Imran Khan
University of Maryland, College Park
15 PUBLICATIONS **483** CITATIONS
SEE PROFILE

Materials Science & Engineering C 91 (2018) 436–444

Contents lists available at ScienceDirect

Materials Science & Engineering C

journal homepage: www.elsevier.com/locate/msec

Biosynthesis of magnesium oxide (MgO) nanoflakes by using leaf extract of *Bauhinia purpurea* and evaluation of its antibacterial property against *Staphylococcus aureus*

Bhaskar Das[a], Sahoo Moumita[b], Soumen Ghosh[c], Md Imran Khan[c], Dash Indira[b], R. Jayabalan[b], Suraj K. Tripathy[c], Amrita Mishra[c], P. Balasubramanian[a,*]

[a] Bioenergy and Environmental Laboratory, Department of Biotechnology & Medical Engineering, National Institute of Technology, Rourkela, Odisha 769008, India
[b] Food Microbiology and Bioprocess Laboratory, Department of Life Science, National Institute of Technology, Rourkela, Odisha 769008, India
[c] School of Biotechnology, KIIT University, Bhubaneswar, Odisha 751024, India

ARTICLE INFO

Keywords:
Nanoflakes
Biocompatibility
Bauhinia purpurea
Staphylococcus aureus
Antibacterial agents
Magnesium oxide

ABSTRACT

Nanobiotechnology has become a newly evolving field of interest in biomedical applications due to its biocompatibility and non-toxic nature towards the environment. Metal and metal oxide nanoparticles have been widely used as an antibacterial agent due to the emergence of antibiotic resistant pathogens, which leads to the outbreak of infectious diseases. In the present paper, biogenic synthesis of magnesium oxide (MgO) nanoflakes is reported by using *Bauhinia purpurea* leaf extract through alkaline precipitation method along with its detailed characterization. The average size of synthesized nanoflakes was found to be around 11 nm. Electron microscopy was used to investigate the morphology of the MgO nanoflakes. Additionally, the presence of antioxidants, phenolics and flavonoids in *B. purpurea* leaf extract has been studied by using different assays, which suggested the efficacy of leaf extract as a potential reducing agent for MgO nanoflakes synthesis. Antibacterial activity of synthesized MgO nanoflakes was investigated against *Staphylococcus aureus*, a gram positive bacteria known to cause various infections in humans. Results suggested the high efficacy of MgO nanoflakes as a potential antibacterial agent against *S. aureus* at meager dose size (250 μg/ml) and possible mode of action was investigated through surface morphology analysis of bacterial cells by field emission scanning electron microscopy.

1. Introduction

For the last few years, antibiotics have been used widely to control infections related to community and hospital environment [1]. Continuous exposure to antibiotics is one of the main reasons behind the emergence of antibiotic resistant microbes with high pathogenicity, which leads to the occurrence of deadly infectious diseases out bursting worldwide [2]. Most of the time, out of these pathogenic microorganisms, bacteria have shown more susceptibility towards this antibiotic resistance phenomenon due to their adaptive environmental conditions based manipulative gene features. Among these pathogenic bacterial strains, *Enterococcus*, *Streptococcus* and *Staphylococcus* are common and closely related species which can cause a wide variety of infections and diseases [3]. Development and industrialization of human population have contributed majorly in epidemic outbreaks of various bacterial infections around the world where, incidence of *S. aureus* infection ranges from 10 to 30 per 100,000 persons per year [4]. *S. aureus* is one of the common human pathogens which is mainly responsible for local infections such as wound and postoperative infections and also for prosthetic infections related to endotracheal tubes and other biomaterials [5]. *S. aureus* has also shown the ability to resist the common antibiotics such as penicillin, methicillin, tetracycline, erythromycin, and vancomycin [6,7]. Among all of these, methicillin-resistant *S. aureus* (MRSA) has become endemic in India. The incidence of infectious outbreaks varies from 25% to 50% in western part of India and South India, respectively [8,9]. Despite the use of several antibacterial therapies, the morbidity and mortality rate is still high since these broad spectrum drugs hasten the evolution of antibiotic resistant strains of these pathogens. Hence, finding suitable antibacterial agents as well as strategies have become a hot topic of research.

Antibacterial agents, excluding antibiotics, have a wide variety of fields of applications such as water disinfection, textile industries, food packaging and most importantly in medical science [10]. Various organic and inorganic materials have been tested as an antibacterial agent which possess some disadvantages including high toxicity and cost effectiveness. Nanomaterials are at the prominent edge of the hastily

* Corresponding author.
E-mail addresses: jayabalanr@nitrkl.ac.in (R. Jayabalan), biobala@nitrkl.ac.in (P. Balasubramanian).

https://doi.org/10.1016/j.msec.2018.05.059
Received 6 September 2017; Received in revised form 22 March 2018; Accepted 17 May 2018
Available online 18 May 2018
0928-4931/

developing field of nanotechnology. Due to its small size, large surface to volume ratio and other prime novel characteristics, the nanoparticle has shown some outstanding, promising results regarding the applications as an antibacterial agent. The ability to prepare metal and metal oxide nanoparticles of specific size and shape may likely lead to the development of new antibacterial agents [11]. Various reports have been published demonstrating the effectiveness of different metal nanoparticles like gold (Au), silver (Ag) and metal oxide nanoparticles like zinc oxide (ZnO), titanium dioxide (TiO_2), copper oxide (CuO), magnesium oxide (MgO) in the field of biomedical applications [12–13]. Metal oxide nanoparticles having different band gap energy makes them useful for various catalytic applications acting as a semiconductor. Researchers have proved that this phenomenon can also be used in evaluating the antibacterial efficacy of metal oxide nanoparticles [14–16]. Additionally, out of all the metal oxide nanoparticles, MgO nanoparticles has been well studied for antibacterial activities [17]. Leung et al. (2014) [18] described that strong antibacterial activity of the MgO nanoparticles could be observed in the absence of any reactive oxygen species (ROS) production. They declared that the mechanism of antibacterial activity might be due to the cell membrane damage. Although chemically synthesized metal oxide nanoparticles have shown the greatest potential for killing pathogenic bacteria, there are huge disadvantages due to its toxicity towards our environment [19]. Biological methods provide a broad range of resources for the synthesis of nanoparticles. Additionally, three valuable advantages of synthesis of biogenic nanoparticles are widely accepted in the research community. Firstly, due to its eco-friendly approach where the use of biodegradable substances for the synthesis of nanoparticles possesses non-toxic effect on the environment and thereby leads to a green technological approach. Secondly, cost effectiveness of the synthesis protocol where the use of biological substances which are easily available makes it more reliable and sustainable technology. Thirdly, the biocompatible character of the synthesized biogenic nanoparticles has more impact than the conventional chemically synthesized nanoparticles [20].

Keeping this in view, in the present study, we have synthesized MgO nanoflakes by using the leaf extract of *B. purpurea* which belongs to the family of Fabaceae and commonly known as purple camel's foot. It has well known medicinal properties which have been used to treat several ailments in traditional medicine [21]. Biosynthesized MgO nanoflakes were characterized by using UV–visible spectrophotometry, Fourier Transform Infrared Spectroscopy (FTIR), Field Emission Scanning Electron Microscopy (FESEM), Transmission Electron Microscopy (TEM), and other characterization techniques. The efficiency of *B. purpurea* leaf extract as a reducing agent for the synthesis of MgO nanoflakes was determined by using free radical scavenging activity assays and reduction potential evaluation of the leaf extract solution. After that, the antibacterial property of MgO nanoflakes was determined against *S. aureus* using colony forming unit (CFU) assay and UV–visible spectrophotometric analysis. Finding the antibacterial mechanism was carried out by surface morphology changes in FESEM analysis.

2. Experimental

2.1. Preparation of leaf extract (bio-reductant)

B. purpurea plant leaves were collected from the campus of National Institute of Technology (NIT) Rourkela, Odisha, India during November 2016. A solution was prepared by grinding 10 g of leaves in 100 ml of distilled water. The first solution was passed through a muslin cloth, and the filtrate was filtered twice using filter paper (Whatman Filter paper No 1). The prepared extract solution was then centrifuged at 5000 rpm at 25 °C for 15 min. The filtrate was used as a stock solution for the synthesis of MgO nanoflakes (the plant extract was processed and prepared fresh for every experiment performed during the study).

2.2. Biosynthesis of MgO nanoflakes

For MgO nanoflakes synthesis, 90 ml of $MgCl_2$ (1 mM) was added to 10 ml of plant extract (prepared from *B. purpurea* plant) and kept on stirring condition at 600 rpm at 90 °C. After reaching the desired temperature, 2 M NaOH solution was added to the reaction mixture drop wise. The precipitate was formed after adding the alkaline solution. An aliquot was taken from the cloudy solution for spectrophotometric analysis. The reaction solution was kept for 3 h for the ageing process. After that cloudy solution containing MgOH was centrifuged at 7500 rpm at 25 °C for 20 min and the pellet was washed twice with ethanol (99%). Pellets were air dried and then calcinated at 550 °C for 5 h in a muffle furnace.

2.3. Characterization of biogenic MgO nanoflakes

The synthesis of MgO nanoflakes was followed by UV–visible spectrophotometric analysis (Agilent Technologies, Cary series UV–vis spectrophotometer, USA). Biosynthesized and purified nanoparticles were further characterized by different instrumental techniques. The surface morphology of the nanoparticles was investigated by field emission scanning electron microscopy (FESEM, Nova nanoSEM 450, Czech Republic) and the structure was determined using transmission electron microscopy (TEM-TECNAI TF 30 G2 SUPER TWIN by FEI, USA). The crystal structure of the materials was investigated by X-ray diffraction technique (XRD, D/Max 2005, Rigaku, Japan). For detection of surface functional groups, the synthesized MgO nanoflakes were characterized using Fourier transform infrared spectrophotometer (FTIR; Shimadzu 8201PC, Japan). Surface charge or Zeta potential (Zp) of MgO nanoflakes was measured by dynamic light scattering techniques (DLS, Zetasizer Nano ZS90, Malvern, UK).

2.4. Free radical scavenging activity and antioxidant potential of B. purpurea leaf extract

2.4.1. DPPH scavenging ability

DPPH scavenging ability was determined according to the method reported by Blois (1958) [22] with minor modifications. 200 µl leaf extract was mixed with 2 ml of 0.1 mM DPPH in ethanol solution and 800 µl of 50 mM Tris-HCl buffer (pH 7.4). The solutions were incubated at room temperature for 30 min, and reduction of DPPH free radical was measured by reading the absorbance at 517 nm. Ascorbic acid (1 mg/ml) solution was taken as the standard, and the tube without sample was considered as a control solution [23]. This is represented as % DPPH radical scavenging activity and is calculated using Eq. (1).

$$DPPH\ scavenging\ activity\ (\%) = \frac{Control\ absorbance - Sample\ absorbance}{Control\ absorbance} \times 100 \quad (1)$$

2.4.2. Reducing power assay

Reducing power assay was done by following the protocol described by Yildirim et al. (2001) [24]. *B. purpurea* leaf extract (20 µl) was mixed with 2.5 ml of phosphate buffer (0.2 M, pH 6.6) and 2.5 ml of potassium ferricyanide as outlined in Yang et al. (2008) [25]. The reaction mixture was incubated at 50 °C for 30 min [26]. Subsequently, 2.5 ml of trichloro acetic acid was added and centrifuged at 3000 rpm for 10 min. The upper layer solution (2.5 ml) was mixed properly with 2.5 ml of distilled water and 0.5 ml of ferric chloride. Absorbance was measured at 700 nm. The absorbance of the reaction mixture is directly proportional to the reducing power [23].

2.4.3. Determination of total phenolic content

Total phenolic content was determined spectrophotometrically with Folin-Ciocalteu reagent [27]. *B. purpurea* aqueous leaf extract (2 ml) was mixed with 10 ml of Folin-Ciocalteu diluted reagent (1/10 with

double-distilled deionized water). After 2 min incubation, 8 ml of sodium carbonate was added to the reaction solution. The reaction solutions were then kept in the dark for 2 h at room temperature. The absorbance was measured at 765 nm [23]. A standard curve was prepared using gallic acid with the concentration range from 50 to 500 μg/ml. Results are expressed in μg of gallic acid equivalent (GAE) per ml of *B. purpurea* extract [28].

2.4.4. Total flavonoid content

Total flavonoid content was assessed by the aluminium chloride colorimetric method [29]. One ml of *B. purpurea* leaf extract was mixed with 4 ml of distilled water and then 0.3% of the $NaNO_2$ solution. After 5 min of incubation 0.3%, $AlCl_3$ was added, and the solution was allowed to stand for 6 min. Then 2 ml of 1 mol/l NaOH solution was added, and the final volume of the reaction mixture was made up to 10 ml with distilled water. The mixture was allowed to stand for next 15 min, and the absorbance was taken at 570 nm. The total flavonoid content was calculated from the calibration curve, and the result was expressed as mg catechin equivalent per g dry weight [30].

2.5. Antibacterial activity of MgO nanoparticles

2.5.1. Preparation of bacterial culture solution

Bacterial strain *S. aureus* MTCC-3384 (Gram-positive) was collected from Microbial Type Culture Collection and Gene Bank (MTCC) Chandigarh, India. The strain was revived and subcultured at 37 °C in nutrient broth under shaking condition (150 rpm). After full growth of the bacterial stock solutions, it was kept at 4 °C for further antibacterial analysis. Subculturing has been done before the antibacterial experiment.

2.5.2. Colony forming unit (CFU) assay

Antibacterial activity of MgO nanoparticles was studied against the pathogenic strain of *S. aureus* MTCC-3384 (Gram-positive) using CFU assay. The freshly subcultured bacterial culture was prepared before starting the experiment. CFU assay was performed by inoculating 100 μl of fresh bacterial culture (1.0×10^7 CFU/ml) with different concentration of MgO nanoflakes (0, 100, 250, 500, 750, and 1000 μg/ml) and the final volume of the reaction set up was made up to 5 ml. For control, the MgO nanoflakes solution was not added to the reaction media. The experiment was carried out for 8 h and aliquots were taken in every 1 h interval, and all the samples were plated on nutrient agar to check the colony forming units (CFU) and growth inhibition pattern. Additionally, minimum inhibitory concentration (MIC) value of MgO nanoflakes was determined considering the lowest concentration of materials which could inhibit the growth of *S. aureus*.

2.5.3. Evaluation of antibacterial activity of MgO nanoflakes using spectrophotometric analysis

The spectrophotometric analysis was done by using UV–vis spectrophotometer (Agilent Technologies, Cary series UV–vis spectrophotometer, USA). The experimental pattern was followed in a similar manner of CFU assay, but in 50 ml (nutrient broth) reaction set up. The reaction was carried out for 8 h and spectrophotometric analysis was done in every 1 h interval to determine the optical density (OD value) at 600 nm to investigate the growth pattern of the bacteria in the presence of MgO nanoflakes with different concentration as followed in CFU assay.

2.5.4. FESEM analysis for the antibacterial mechanism of MgO nanoflakes

FESEM analysis was also done for determining the morphological changes of the bacterial colony during the nanoparticles and bacterial interaction which leads to growth inhibition of bacteria. Bacteria were treated with MgO nanoflakes with the MIC concentration, i.e., 250 μg/ml (MIC concentration of MgO from CFU assay). FESEM slides were prepared by taking 0 h, and 8 h sample (from spectrophotometric analysis) and the standard protocol was followed for FESEM slide preparation as outlined in Song et al. (2011) [31].

2.5.5. Investigation of viability of S. aureus through fluorescence microscope

Live/dead staining was performed to investigate the viability of *S. aureus* after treating it with different concentration of MgO nanoflakes. Assay has been done according to manufacturer protocol (LIVE/DEAD™ BacLight™ Bacterial Viability Kit, Invitrogen™). *S. aureus* cells were incubated with different concentrations (control, 100, 250, 500, 750 and 1000 μg/ml) of MgO nanoflakes for 4 h and 8 h, respectively. Culture media was discarded followed by centrifugation and the pellet was washed using 1× PBS followed by resuspension in it. Then SYTO9 and propidium iodide (PI) was added into treated and control (untreated) samples followed by its incubation at room temperature for 15 min under dark condition. Results were analyzed under fluorescence microscope (Life Technologies, USA) at 40× magnification.

2.5.6. Analysis of reactive oxygen species in MgO nanoflakes treated S. aureus

Intracellular reactive oxygen species (ROS) was qualitatively measured using DCF-DA (2′,7′-Dichlorofluorescin diacetate) under fluorescence microscope [32]. DCF-DA is a particular dye which enter into the cells inertly and counters with ROS to form greatly fluorescent dichlorofluorescein. In the present work, 1 ml overnight grown culture of *S. aureus* was treated with MgO nanoflakes (control, 250, 500, 750 and 1000 μg/ml) centrifuged and washed with 1× PBS followed by resuspension in it. Further, 10 μM of DCF-DA was added and incubated under dark condition for 15 min at 37 °C. Results were analyzed through fluorescence microscope (Life Technologies, USA) 40× magnification.

3. Results and discussion

3.1. Synthesis and characterization of MgO nanoflakes

3.1.1. UV-visible spectroscopy

Biosynthesis of MgO nanoflakes has been followed by the change in the color of the reaction solution assisted by the *B. purpurea* leaf extract through precipitation method. The color of the solution changed from colorless to a cloudy brown solution which suggests a probable synthesis of MgO and MgOH complex in the solution. The adsorption spectrum of MgO particles was recorded within the range of 200–800 nm. Fig. 1 shows the UV spectrum of MgO nano flakes, in which a slightly intense peak observed around 270 nm, confirmed the synthesis of nanosized MgO particles [33]. Additionally, precursor salt solution for the synthesis of MgO, i.e., magnesium chloride ($MgCl_2$) has not shown any surface plasmon resonance (SPR) band as compared to the MgO nanoflakes solution synthesized by *B. purpurea* leaf extract. Due to the presence of free surface electrons, metal and metal oxide nanoparticles show surface SPR band in the UV–visible spectrum. Thus slightly intense SPR band around 280–290 nm could be attributed to the synthesis of metal oxide nanoparticles after addition of the leaf extract and NaOH solution. This interesting optical phenomenon is associated with the formation of MgO nanoparticles from its precursor salt solution.

3.1.2. XRD

Phase and crystal structure of the biologically synthesized MgO nanoflakes have been investigated by X-ray diffraction technique for better understanding of the positions of its atoms in the lattice structure. Fig. 2 shows the corresponding XRD pattern of the MgO nanoflakes powder. Two clear and distinct principal/major peaks (at $2\theta = 42.823, 62.169$) and two minor peaks (at $2\theta = 38.47, 78.50$) obtained correspond to (200), (220), and (222), (111) planes of MgO are having a face centered cubic bravis lattice structure. The conformity of the result is verified and was found to correspond accurately to the

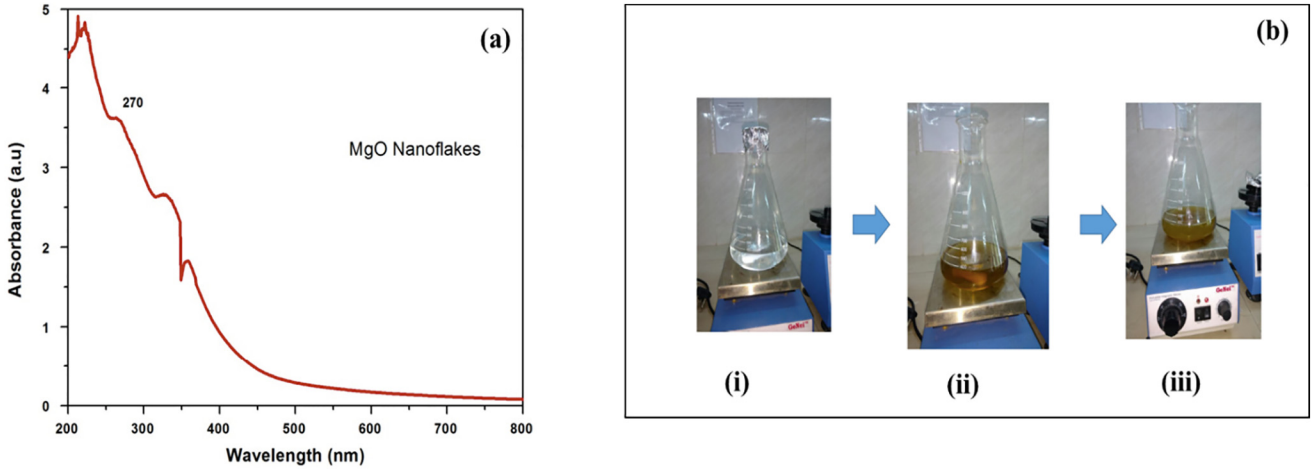

Fig. 1. (a) UV–vis spectrum of biologically synthesized MgO nanoparticles using *B. purpurea* leaf extract, (b) Visual observation of MgO nanoflakes synthesis procedure (i) 10 mM $MgCl_2$ aqueous solution with continuous stirring, (ii) After addition of the plant extract the colour of the solution changed to light brown, (iii) Finally, addition of 2 M NaOH solution (drop wise) changed the colour of the solution to cloudy brown. (For interpretation of the references to colour in this figure legend, the reader is referred to the web version of this article.)

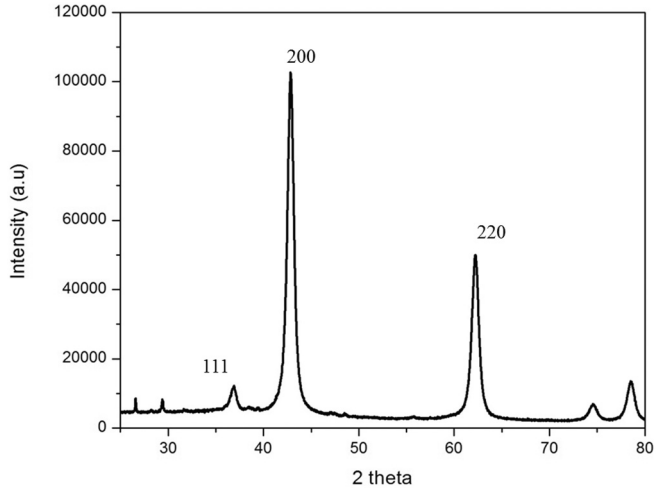

Fig. 2. XRD analysis of MgO nanoflakes synthesized by *B. purpurea* leaf extract.

standard XRD data JCPDS card (No: 78-0430). No significant characteristic peaks of Mg and other impurities are detected in the pattern which indicates the high purity of the synthesized MgO nanoflakes. Mean crystallite diameter (D) have been calculated using Scherrer's formula (Eq. (2)) for (200), and (220) planes and is calculated to be 11.4 nm [34–35].

$$D = \frac{K\lambda}{\beta \cos\theta} \tag{2}$$

where, K is the dimensional constant depending on the particular geometry of the scattering object, λ is the wavelength of the X-ray radiation, β is the full width at half maximum (FWHM) of the principal/major peak in radian and θ is the Bragg's angle of the line profile correlating to half of the exact position of the principal peak.

3.1.3. Investigation of structural morphology and surface charge

3.1.3.1. FESEM. Morphology and compositional analysis of biologically synthesized MgO nanoflakes using *B. purpurea* leaf extract was done by using electron microscopy. Fig. 3(a) shows the field emission scanning electron microscopy (FESEM) image of MgO nanoparticles, which exhibit flakes-like structure due to the aggregation of several thousand MgO nanoparticles. The MgO nanoflakes are dense and interconnected with each other such that no clear boundaries exist between one another.

3.1.3.2. TEM. Fig. 3(b,c) shows the bright field and scanning transmission electron microscope (STEM) images of MgO nanoparticles which further confirms the flakes-like structure of the MgO nanoparticles and the transparent features suggest that the nanoflakes are very thin. High Resolution TEM (HR-TEM) images are shown in Fig. 3(d,e) and the material is found to have inter planner spacing of ~0.234 nm, which is close to the (111) plane of MgO with a cubic structure. Fig. 3(f) shows the selected area diffraction pattern (SAED) of individual MgO nanoflake showing three distinct discernible diffraction rings which confirm the presence of polycrystalline nature and can be indexed to the cubic phase of MgO [36]. TEM Energy Dispersive X-ray Spectrometry (EDS) is used to understand the chemical composition of the nanoparticles. As shown in Fig. 4(a), MgO has shown a clear peak corresponding to Mg and O. Additionally peaks of C and Cu are also obtained, which may confirm the copper grid and carbon film on which nanoparticles were deposited for TEM studies [37]. Fig. 4(b) shows the High Angle Annular Dark Field (HAADF) images of MgO nanoflakes synthesized by *B. purpurea* leaf extract. The HAADF images taken from an individual cluster of MgO nanoflakes can be seen in Fig. 4(b), where traces of Mg and O_2 can be found independently in a cluster of MgO nanoflakes confirming the presence of MgO in the synthesized nanoflakes. The surface charge of the synthesized MgO nanoflakes was investigated by Zeta potential analysis Fig.4(c), the surface charge of the MgO nanoflakes was found to be +2.70 mv which confirmed the presence of positive charge on the surface of MgO nanoflakes. This positively charged MgO nanoflakes can be used as a potential antibacterial agent due to its affinity towards the negatively charged bacterial cell membrane [38].

3.1.3.3. FTIR. FTIR analysis was done to investigate the absorbed molecules and/or functional groups on the surface of MgO nanoflakes synthesized by *B. purpurea* leaf extract. Additionally, it also contributes to the investigation of the probable synthesis mechanism of MgO nanoflakes in the presence of biological substances. Fig. 5. shows the FTIR spectra where the complex nature of the peaks are expected due to the presence of many biological molecules in the system. There is a slight change in the transmittance intensity of the peaks in two different systems (*B. purpurea* leaf extract and MgO synthesized by *B. purpurea* leaf extract). In Fig. 5, FTIR spectra of leaf extract and MgO nanoflakes both showed strong bands at 3200–3800, 3600, 2920, 1507, 1017, 810 cm^{-1} and 1994, 1545, 1005, 795 cm^{-1}, respectively. In particular,

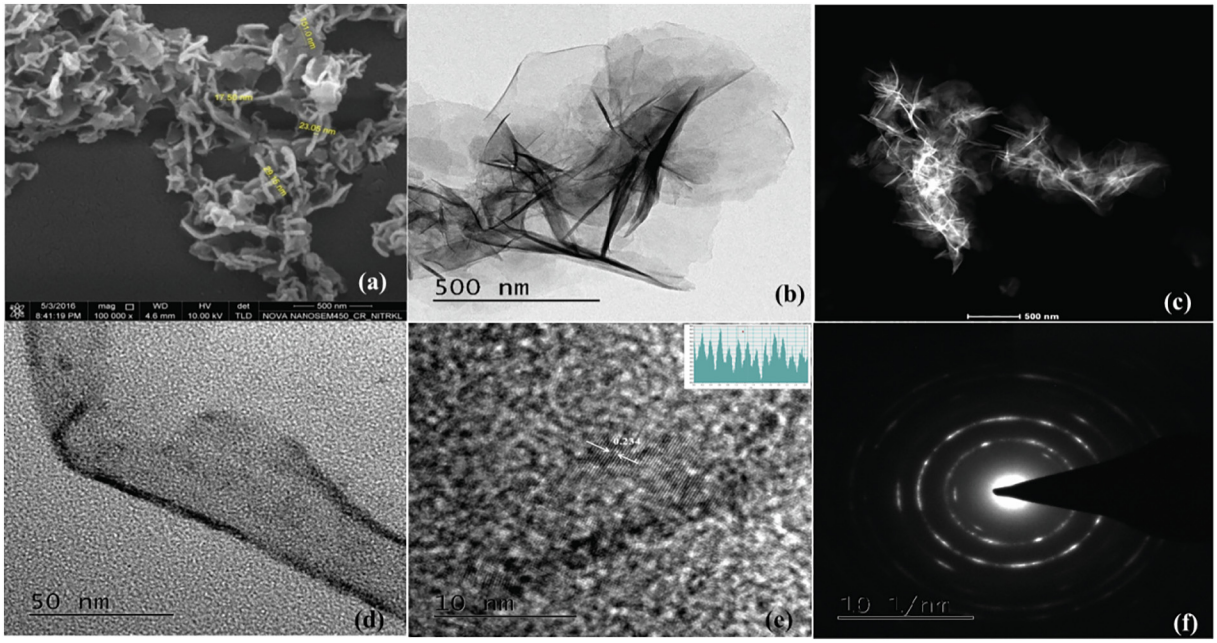

Fig. 3. (a) Field emission Scanning electron microscopy (FESEM) images of synthesized MgO nanoflakes. Transmission electron microscopy (TEM) images (b) Bright field images; (c) STEM; (d) & (e) HRTEM images; (f) SAED pattern, respectively of MgO nanoflakes.

there is a broad peak in the range of 3200–3800 cm^{-1} which may correspond to the stretching vibration of OH or NH groups. Bands appeared at 3660 and 2920 cm^{-1} are corresponding to sharp stretching of OH (alcohol) and aliphatic C—H stretching. Intense peak at 1994 cm^{-1} in MgO nanoflakes corresponds to C—H bending of aromatic compounds which can be correlated to changes occurring in the biological molecules during synthesis of MgO nanoflakes from its precursor salt solution. There are few slightly intense peaks around

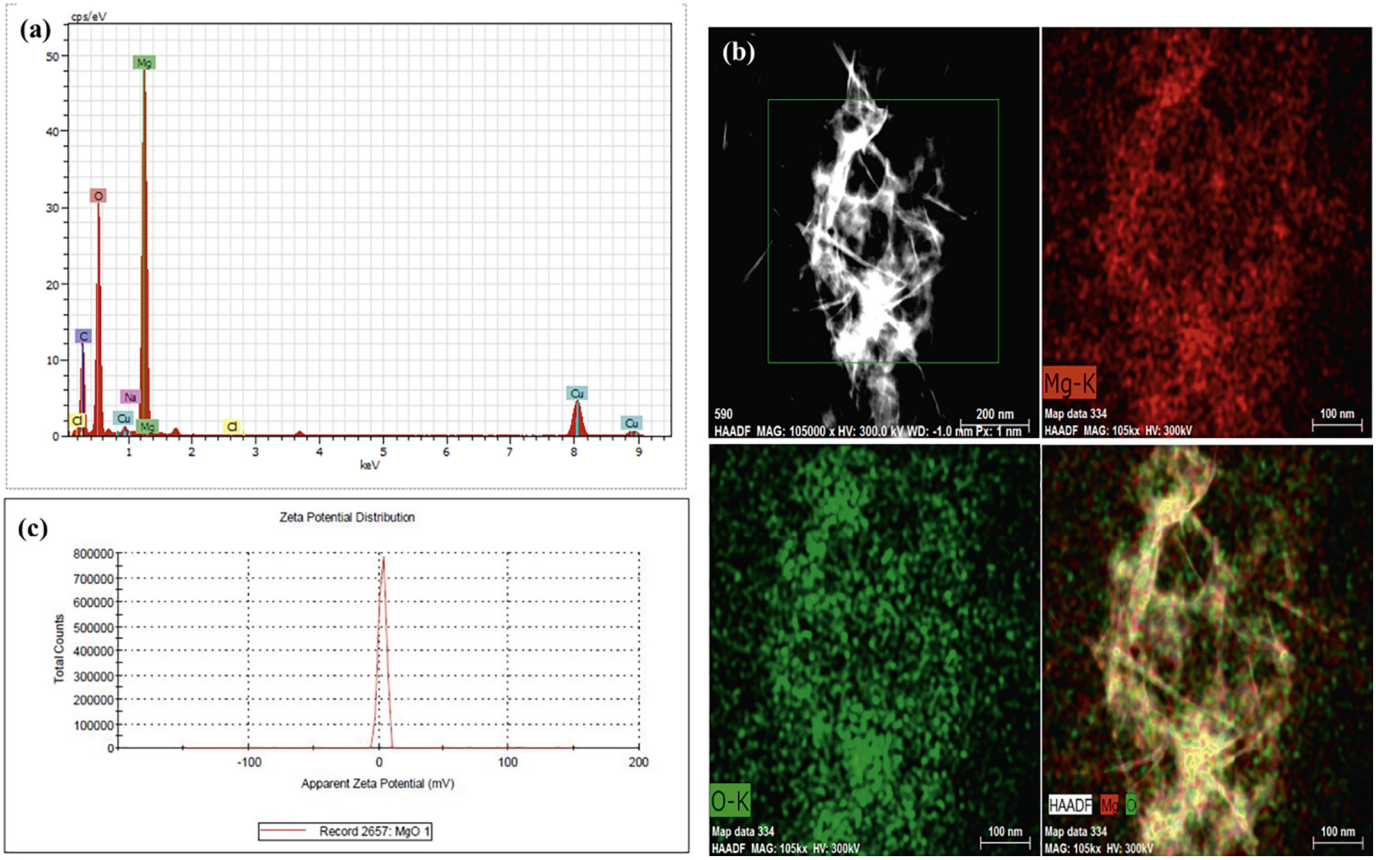

Fig. 4. (a) EDAX analysis of synthesized MgO nanoflakes; (b) HAADF images of MgO nanoflakes; (c) surface charge analysis/Zeta potential of biologically synthesized MgO nanoflakes by using *B. purpurea* leaf extract.

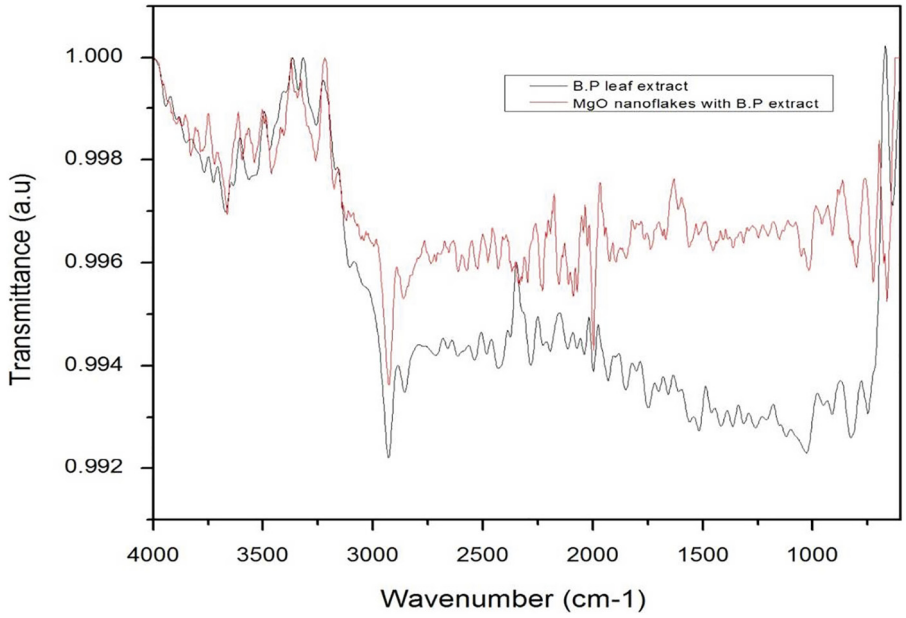

Fig. 5. FTIR spectra of MgO nanoflakes synthesized by using *B. purpurea* leaf extract.

1507 and 1545 cm^{-1} in both the samples representing stretching of N—O nitro compounds. The bands at 1017 and 1005 cm^{-1} corresponds to C—N stretching vibration of aliphatic amines. The peaks near 600–800 cm^{-1} attributed to R-H groups where 658 cm^{-1} corresponds N—H wags of primary and secondary amine in the synthesized material (MgO). Hence, the presence of some biological main components such as steroids, saponins, tannins, phenolics, flavonoids, and glycosides in the leaf extract of *B. purpurea* can be inferred from this FTIR spectrum which have assisted the synthesis of MgO nanoflakes by reducing and capping of the Mg^{2+} ion under alkaline condition.

3.2. Free radical scavenging activity and antioxidant potential of B. purpurea leaf extract

3.2.1. DPPH scavenging ability

Antioxidant activity of an aqueous leaf extract of *B. purpurea* measured by DPPH method (517 nm) is shown in Table 1. The antioxidant activity of aqueous leaf extract exhibited a moderate inhibition of DPPH with 34.32 ± 0.55% RSA (Radical Scavenging Activity) as compared to ascorbic acid which showed around 72.22 ± 0.22% inhibition of DPPH.

3.2.2. Reducing power assay

Reducing power assay was done to determine the electron donating ability of the complex compounds present in the extract samples, which would lead to the reduction of Mg^{2+} ions to its nanoparticle form. Table 1 represents the reducing power ability of the aqueous leaf extract solution in comparison with ascorbic acid as a standard. It can be seen that the absorbance value of *B. purpurea* leaf extract solution is around 0.128 ± 0.33 which are less as compared to that of ascorbic acid (i.e., 0.300 ± 0.03), which indicates the mild reduction potential of *B. purpurea* leaf extract.

3.2.3. Determination of total phenolic content

Total phenolic content was determined spectrophotometrically (765 nm) by taking gallic acid as standard. Gallic acid standard curve was made for the calculation of the actual amount of phenolic compounds present in the leaf extract. Total phenolic content of the *B. purpurea* aqueous leaf extract was found to be 31.83 ± 0.56 GAE per ml. It can be inferred from Table 1 that the amount of phenolic content present in the leaf extract sample may be responsible for the reduction of Mg^{2+} ions to form MgO nanoflakes.

3.2.4. Total flavonoid content

Total flavonoid content was measured by aluminium chloride method at 510 nm in a spectrophotometer. Total flavonoid content of the aqueous *B. purpurea* leaf extract was found to be 311.93 ± 0.25 μg CE (catechin equivalent) per ml (Table 1). Flavonoids, including flavones, flavonols and condensed tannins, are secondary metabolites of plants, the antioxidant activity of which depends on the presence of free OH groups, especially 3-OH. Plant flavonoids have antioxidant activity in vitro and also act as antioxidants in vivo.

From the above study of free radical scavenging activity and antioxidant potential of *B. purpurea* leaf extract solution, it can be inferred that the *B. purpurea* leaf extract is having a higher amount of flavonoid content and a moderate level of phenolic and antioxidant content. The presence of these biological molecules is probably responsible for the bioactivity of the extract, [39] which leads to the reduction of $MgCl_2$ salt solution to form MgO nanoflakes.

Table 1
Free radical scavenging activity and antioxidant potential of *B. purpurea* leaf extract.

Sample	Free radical scavenging activity and antioxidant potential of *B. purpurea* leaf extract			
	DPPH scavenging ability (%)	Reducing power (absorbance)	Toal phenolic content (μg GAE $ml^{-1)}$	Total flavonoid content (μg CE ml^{-1})
B. purpurea aqueous leaf extract	34.32 ± 0.55	0.128 ± 0.33	31.83 ± 0.56	311.93 ± 0.25
Ascorbic acid	72.22 ± 0.22	0.300 ± 0.03	–	–

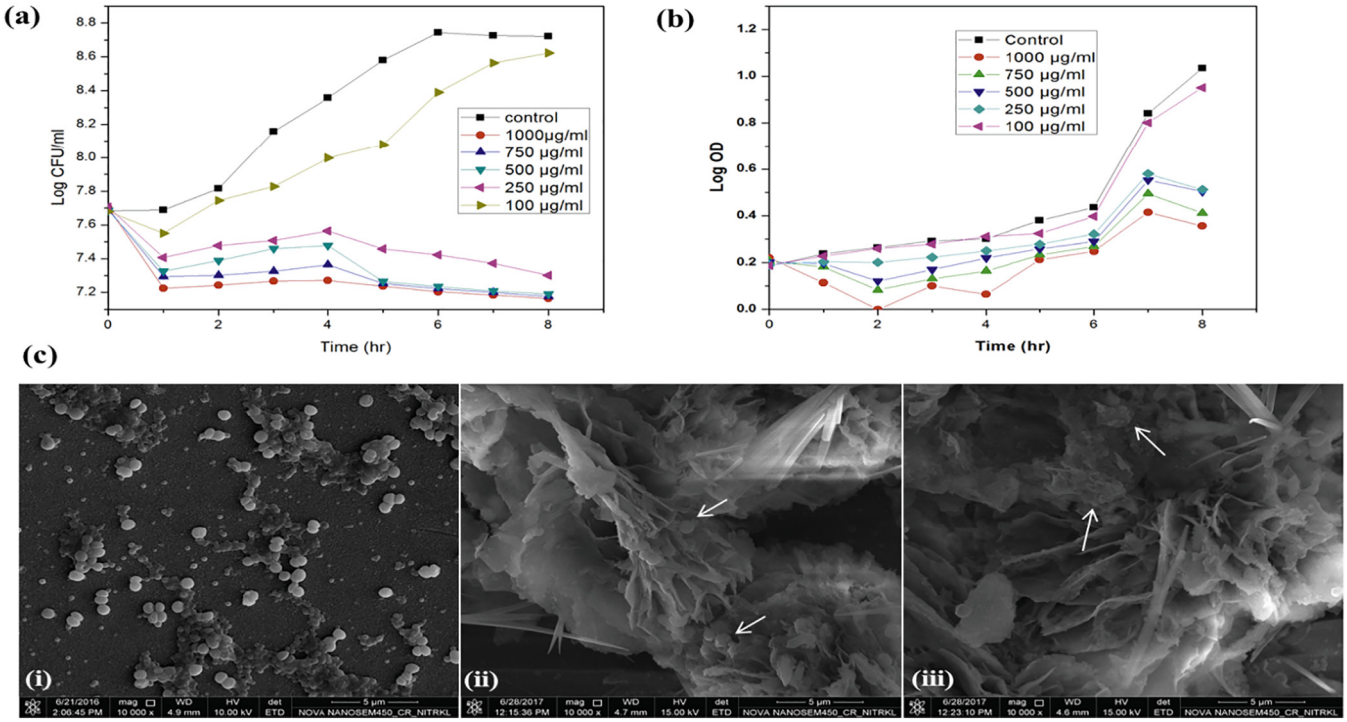

Fig. 6. Antibacterial activity of MgO nanoflakes against *S. aureus* (MTCC-3384). (a) Colony forming Unit (CFU) assay at different concentration of MgO nanoflakes; (b) Spectrophotometric analysis of antibacterial activity of MgO nanoflakes against *S. aureus*; (c) FESEM images of bacteria and MgO nanoflakes (250 µg/ml) interaction at different time interval (i) Control (ii) 0 h (iii) 8 h. For this experiment *S. aureus* cells were incubated with 250 µg/ml of MgO nanoflakes.(arrows suggesting the presence of bacterial cells).

3.3. Antibacterial activity of MgO nanoparticles

3.3.1. Colony forming unit/CFU assay

The antibacterial activities of biologically synthesized MgO nanoflakes using *B. purpurea* leaf extract was investigated against *S. aureus* MTCC-3384 (Gram-positive) by treating the pathogen with different concentrations of MgO nanoflakes (0,100, 250, 500, 750, and 1000 µg/ml) and the effectiveness of the nanomaterials were calculated through colony forming unit (CFU) assay by plating the treated sample on nutrient agar. Fig. 6(a) shows the antibacterial activity of MgO nanoflakes at different concentrations. The graphical representation of antibacterial activity against *S. aureus* (Fig. 6a) shows the $\log_{10}$ CFU value of bacteria with different nanomaterial concentration at various time interval till 8 h incubation. It can be observed that MgO nanoflakes at a concentration of 500, 750 and 1000 µg/ml have completely inhibited the growth of *S. aureus* following 8 h incubation. The MIC value for synthesized MgO nanoflakes is taken as 250 µg/ml because at a lower concentration of nanomaterials the antibacterial efficacy of the materials became less. From Fig. 6(a) it is observed that after decreasing the concentration of nanoflakes from 250 to 100 µg/ml and then to 0 µg/ml (control) the antibacterial activity decreased. Earlier reports with chemically synthesized MgO nanoparticles have shown the MIC value of their material to be 625 µg/ml against *S. aureus* [40].

3.3.2. Evaluation of antibacterial activity of MgO nanoflakes using spectrophotometric analysis

Fig. 6(b) shows the spectrophotometric analysis of the antibacterial activity of biologically synthesized MgO nanoflakes against *S. aureus* MTCC-3384 (Gram-positive). Fig. 6(b) represents $\log_{10}$ OD (Optical Density) values of testing pathogen under different concentration (0, 100, 250, 500, 750, and 1000 µg/ml) of MgO nanoflakes at various time interval. It can be seen that the growth of *S. aureus* at different concentrations of MgO nanoflakes has followed the same pattern as compared to the CFU assay analysis for antibacterial efficacy determination. Nanomaterials with a higher concentration such as 500, 750, and 1000 µg/ml have shown more growth inhibition, where, below 250 µg/ml, the inhibition efficiency got decreased significantly as compared to the control. Thus in this study also 250 µg/ml has been taken as a minimum inhibitory concentration (MIC) value of MgO nanoflakes to act as an effective antibacterial agent.

3.3.3. FESEM analysis for the antibacterial mechanism of MgO nanoflakes

The morphological changes in bacterial cells due to the action of MgO nanoflakes was determined by FE-SEM. Micrographs of the untreated and treated cells have been shown in the Fig. 6c (i–iii). It was observed from Fig. 6c (i) that the cells of *S. aureus* are in intact form and having a smooth surface. Fig. 6c (ii, iii) shows the presence of bacterial cells on the surface of biologically synthesized MgO nanoflakes in 0 h and 8 h, respectively. However, at 0 h (Fig. 6c ii) cells are likely to be present in intact condition with the considerably smooth surface. Fig. 6c (iii) shows surface morphology modulation of 8 h treated cells. It shows the deformation of cell structure and clustering of cells with breaks in the cell membrane. Growth inhibition of *S. aureus* might be due to the damage of cell membrane resulting in leakage of intracellular compounds leading to complete cell disruption [41,18]. Hence, from the FESEM images, it can be concluded that MgO nanoflakes (250 µg/ml) have shown a significant alteration in the surface morphology of the bacterial cells which leads to the death of the bacterial cells and growth inhibition. In the present study, the effectiveness of the biologically synthesized MgO nanoflakes against *S. aureus* is high which could be useful for further application in the medical field.

3.3.4. Investigation of viability of S. aureus through fluorescence microscope

Fluorescence microscope has been implemented to confirm the viability of cells after treatment with MgO nanoflakes. *S. aureus* cells (control and treated) were stained with SYTO9 and PI. PI can only penetrate the cells with damaged/disrupted membranes [42] while in contrast, SYTO9 is a green-fluorescent nucleic acid stain which enters live and dead bacterial

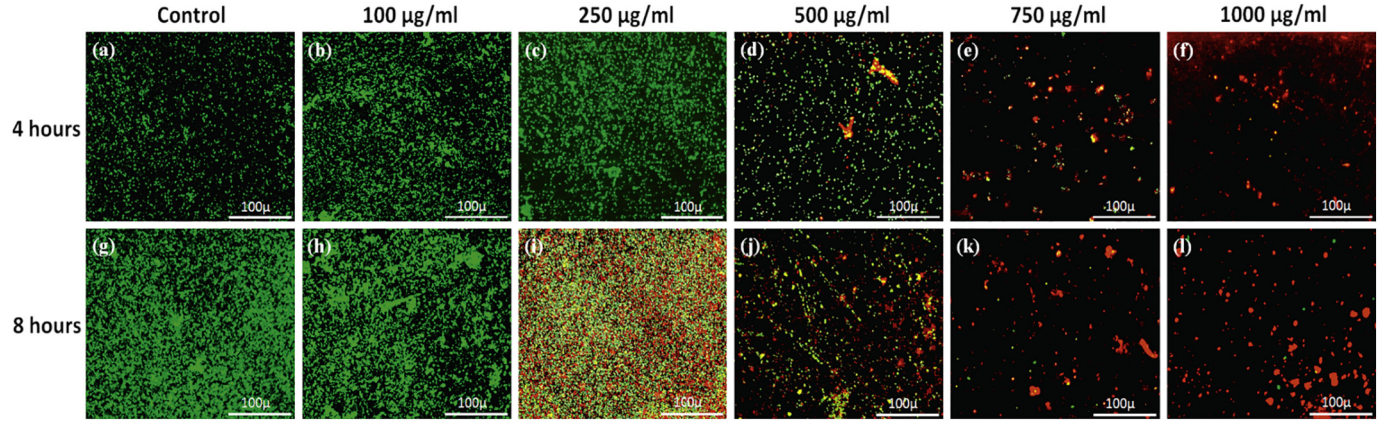

Fig. 7. Qualitative viability of *S. aureus* cells was done through live/dead assay and analyzed under fluorescence microscope. *S. aureus* cells were treated with different concentration of MgO nanoflakes and incubated for 4 h [(a) Control, (b) 100 µg/ml, (c) 250 µg/ml, (d) 500 µg/ml, (e) 750 µg/ml and (f) 1000 µg/ml] and 8 h [(g) Control, (h) 100 µg/ml, (i) 250 µg/ml, (j) 500 µg/ml, (k) 750 µg/ml and (l) 1000 µg/ml]. Two different dyes were used to stain the *S. aureus* cells; SYTO9 (for live cells; which gives green color) and Propidium iodide (dead cells; which gives red color). (For interpretation of the references to colour in this figure legend, the reader is referred to the web version of this article.)

cells. In the presence of both dyes, PI shows a stronger attraction to nucleic acids and latter displaces SYTO9 [43]. Fig. 7(a) shows that there are no dead cells in control sample irrespective of the incubation time, where as in treated samples there was an increase in number of dead cells with increase in the concentration of MgO nanoflakes and incubation time. In the 100 µg/ml treated samples, no dead cells were seen after 4 h and 8 h of incubation (Fig. 7(b) and (h)). Similarly, when *S. aureus* cells were treated with 250 µg/ml nanoflakes, the number of non-viable cells was very less after 4 h (Fig. 7(c)) of incubation. After 8 h of incubation drastic increment in dead cells was observed (Fig. 7 (i)). Interestingly, remarkable results were seen in case of 500, 750 and 1000 µg/ml treated samples. After 4 h of incubation with 500 µg/ml nanoflakes the non-viable cells were less (Fig. 7(d)) but, after 8 h of incubation the number of dead cells increased and the quantity of dead cells was more than live cells (Fig. 7(j)). When cells were incubated with 750 µg/ml nanoflakes, the population of dead cells drastically increased in the sample after 4 h of incubation (Fig. 7(e)) and aggregation of cells was also observed (Fig. 7(k)). Highest MgO nanoflakes concentration (1000 µg/ml) has shown remarkable activity after 4 h of incubation (Fig. 7(f)) and no viable cells were detected after 8 h of incubation (Fig. 7(l)). From this assay it was observed that population of dead cells increased with the rise of concentration and incubation time, and very low viability/growth of *S. aureus* was seen after 8 h of incubation with 250, 500, 750 and 1000 µg/ml of MgO nanoflakes compared to control. The data obtained is similar to CFU data since growth of the bacteria was inhibited within 8 h of interaction of the nanoflakes with *S. aureus*.

3.3.5. Analysis of reactive oxygen species in MgO nanoflakes treated S. aureus

Increase in the oxidative stress and induction of intracellular ROS are very crucial in understanding the probable antibacterial mechanism of nanomaterials. In the present work, our findings suggested that the antibacterial activity of the synthesized MgO nanoflakes against *S. aureus* was ROS dependent. The intracellular production of ROS was qualitatively determined using fluorescence microscope by DCF-DA, by means of hydrogen peroxide (H_2O_2) detection. DCF-DA can easily enter into cells due to its high permeability and gets hydrolyzed by intracellular H_2O_2 in cytoplasm leading to the production of dichlorodihydro-fluorescein (DCFH) carboxylate anion [44]. There was no increment in ROS in case of control after 4 h and 8 h of incubation (Fig. 8(a) and (f)). Generation of ROS was observed in *S. aureus* cells treated with 250, 500, 750 and 1000 µg/ml. As shown in Fig. 8(b), increment in ROS was detected after 4 h of incubation with 250 µg/ml and with the rise of incubation time extraordinary increase in ROS was observed (Fig. 8(g)). Treated (500, 750, 1000 µg/ml) cells after 4 h of incubation (Fig. 8(c), (d), (e))showed generation of intracellular ROS which increased up to two-three fold after 8 h of incubation (Fig. 8(h), (i), (j)) as compared to control (Fig. 8(f)). Fluorescence microscopic images showed increased intracellular ROS levels in cells treated with MgO nanoflakes as compared to control. It is well known that all the metal and metal oxide nanoparticles generate ROS in the reaction system [45–46]. In present study, MgO nanoflakes have generated ROS

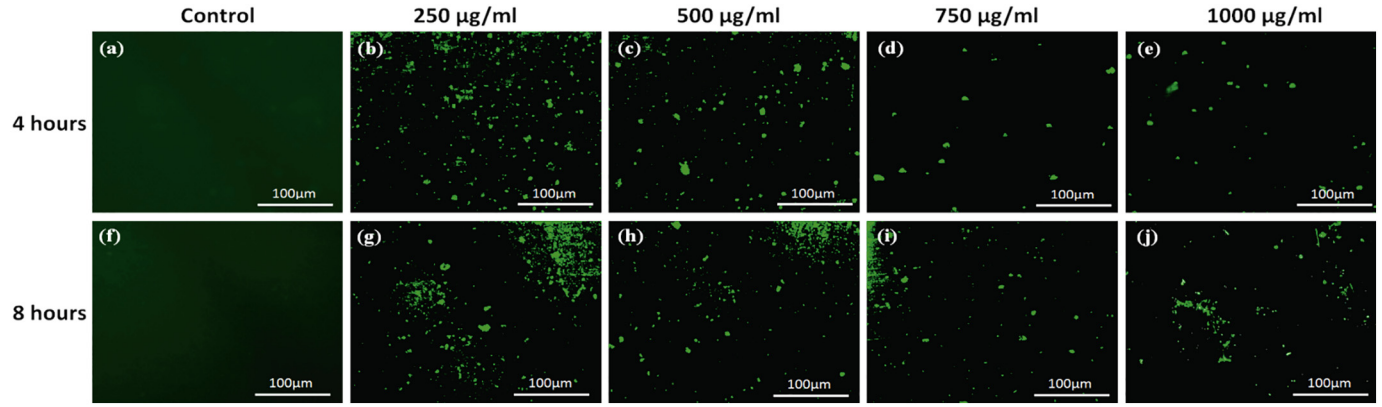

Fig. 8. Antibacterial mechanism of MgO nanoflakes was investigated through measurement of the induction of intracellular reactive oxygen species (ROS) using DCF-DA dye and analyzed under fluorescence microscopy. *S. aureus* cells were treated with different concentration of MgO nanoflakes and incubated for 4 h [(a) Control, (b) 250 µg/ml, (c) 500 µg/ml, (d) 750 µg/ml and (e) 1000 µg/ml] and 8 h [(f) Control, (g) 250 µg/ml, (h) 500 µg/ml, (i) 750 µg/ml and (j) 1000 µg/ml].

in dose dependent manner which may be responsible for its antibacterial activity against *S. aureus*.

4. Conclusion

In summary, the antibacterial activity of biologically synthesized MgO nanoflakes was investigated against *S. aureus* MTCC-3384 (Gram-positive-pathogen). From experimental observations, the present report communicates a likely consequence. MgO nanoflakes were successfully synthesized (10–11 nm) using leaf extract of *B. purpurea* through alkaline precipitation method. The presence of a significant amount of antioxidants, as well as flavonoids and phenolics in the leaf extract of *B. purpurea*, probably assist the biological synthesis of MgO nanoflakes. The antibacterial study indicated the efficacy of MgO nanoflakes at a little dose size (250 μg/ml) than that of the previously reported concentration of MgO nanomaterials and considered as the minimum inhibitory concentration (MIC) for inhibiting the growth of the bacteria. Our investigation suggested that the probable antibacterial mechanism of MgO nanoflakes could be attributed to the production of reactive oxygen species leading to cell membrane damage during the treatment of bacterial cells with MgO nanoflakes. These findings substantiate further studies for possible biomedical applications of this material.

Acknowledgment

The authors thank the Department of Biotechnology and Medical Engineering, Department of Life Science, of National Institute of Technology Rourkela, KIIT school of Biotechnology, KIIT University for providing the research facility. The authors greatly acknowledge the Ministry of Human Resource Development (MHRD) of Government of India for sponsoring the first and second author's doctoral research.

References

[1] J. Davies, D. Davies, Origins and evolution of antibiotic resistance, Microbiol. Mol. Biol. Rev. 74 (3) (2010) 417–433.
[2] U. Desselberger, Emerging and re-emerging infectious diseases, J. Inf. Secur. 40 (1) (2000) 3–15.
[3] N. Jones, B. Ray, K.T. Ranjit, A.C. Manna, Antibacterial activity of ZnO nanoparticle suspensions on a broad spectrum of microorganisms, FEMS Microbiol. Lett. 279 (1) (2008) 71–76.
[4] K.B. Laupland, O. Lyytikäinen, M. Søgaard, K.J. Kennedy, J.D. Knudsen, C. Ostergaard, H.C. Schønheyder, The changing epidemiology of *Staphylococcus aureus* bloodstream infection: a multinational population-based surveillance study, Clin. Microbiol. Infect. 19 (5) (2013) 465–471.
[5] M.C. Hudson, W.K. Ramp, K.P. Frankenburg, *Staphylococcus aureus* adhesion to bone matrix and bone-associated biomaterials, FEMS Microbiol. Lett. 173 (2) (1999) 279–284.
[6] K. Hiramatsu, Vancomycin-resistant *Staphylococcus aureus*: a new model of antibiotic resistance, Lancet Infect. Dis. 1 (3) (2001) 147–155.
[7] H.F. Chambers, The changing epidemiology of *Staphylococcus aureus*? Emerg. Infect. Dis. 7 (2) (2001) 178.
[8] A.K. Patel, K.K. Patel, K.R. Patel, S. Shah, P. Dileep, Time trends in the epidemiology of microbial infections at a tertiary care center in west India over last 5 years, J. Assoc. Physicians India 58 (Suppl) (2010) 37–40.
[9] R. Gopalakrishnan, D. Sureshkumar, Changing trends in antimicrobial susceptibility and hospital acquired infections over an 8 year period in a tertiary care hospital in relation to introduction of an infection control programme, J. Assoc. Physicians India 58 (Suppl) (2010) 25–31.
[10] O. Yamamoto, Influence of particle size on the antibacterial activity of zinc oxide, Int. J. Inorg. Mater. 3 (7) (2001) 643–646.
[11] C.J. Hewitt, S.R. Bellara, A. Andreani, G. Nebe-von-Caron, C.M. McFarlane, An evaluation of the anti-bacterial action of ceramic powder slurries using multi-parameter flow cytometry, Biotechnol. Lett. 23 (9) (2001) 667–675.
[12] O. Mahapatra, M. Bhagat, C. Gopalakrishnan, K.D. Arunachalam, Ultrafine dispersed CuO nanoparticles and their antibacterial activity, J. Exp. Nanosci. 3 (3) (2008) 185–193.
[13] N. Tran, A. Mir, D. Mallik, A. Sinha, S. Nayar, T.J. Webster, Bactericidal effect of iron oxide nanoparticles on *Staphylococcus aureus*, Int. J. Nanomedicine 5 (2010) 277.
[14] S. Das, S. Sinha, B. Das, R. Jayabalan, M. Suar, A. Mishra, ... S.K. Tripathy, Disinfection of multidrug resistant *Escherichia coli* by solar-photocatalysis using Fe-doped ZnO nanoparticles, Sci. Rep. 7 (1) (2017) 104.
[15] S. Das, S. Sinha, M. Suar, S.I. Yun, A. Mishra, S.K. Tripathy, Solar-photocatalytic disinfection of *Vibrio cholerae* by using Ag@ ZnO core–shell structure nanocomposites, J. Photochem. Photobiol. B Biol. 142 (2015) 68–76.
[16] R. Saleh, N.F. Djaja, Transition-metal-doped ZnO nanoparticles: synthesis, characterization and photocatalytic activity under UV light, Spectrochim. Acta A Mol. Biomol. Spectrosc. 130 (2014) 581–590.
[17] J. Vidic, S. Stankic, F. Haque, D. Ciric, R. Le Goffic, A. Vidy, ... B. Delmas, Selective antibacterial effects of mixed ZnMgO nanoparticles, J. Nanopart. Res. 15 (5) (2013).
[18] Y.H. Leung, A. Ng, X. Xu, Z. Shen, L.A. Gethings, M.T. Wong, ... P.K. Lee, Mechanisms of antibacterial activity of MgO: non-ROS mediated toxicity of MgO nanoparticles towards *Escherichia coli*, Small 10 (6) (2014) 1171–1183.
[19] P. Mishra, S. Ray, S. Sinha, B. Das, M.I. Khan, S.K. Behera, ... A. Mishra, Facile biosynthesis of gold nanoparticles by using extract of *Hibiscus sabdariffa* and evaluation of its cytotoxicity against U87 glioblastoma cells under hyperglycemic condition, Biochem. Eng. J. 105 (2016) 264–272.
[20] A. Ingle, M. Rai, A. Gade, M. Bawaskar, *Fusarium solani*: a novel biological agent for the extracellular synthesis of silver nanoparticles, J. Nanopart. Res. 11 (8) (2009) 2079.
[21] H. Manoranjan Sharma, A. Radhapyari Devi, B. Manihan Sharma, Vegetable drugs used by the Meitei community of Manipur, Indian J. Tradit. Knowl. 4 (2005) 42.
[22] M.S. Blois, Antioxidant determinations by the use of a stable free radical, Nature 181 (1958) 1199–1200.
[23] R. Jayabalan, P. Subathradevi, S. Marimuthu, M. Sathishkumar, K. Swaminathan, Changes in free-radical scavenging ability of kombucha tea during fermentation, Food Chem. 109 (1) (2008) 227–234.
[24] A. Yıldırım, A. Mavi, A.A. Kara, Determination of antioxidant and antimicrobial activities of *Rumex crispus* L. extracts, J. Agric. Food Chem. 49 (8) (2001) 4083–4089.
[25] B. Yang, M. Zhao, J. Shi, N. Yang, Y. Jiang, Effect of ultrasonic treatment on the recovery and DPPH radical scavenging activity of polysaccharides from longan fruit pericarp, Food Chem. 106 (2) (2008) 685–690.
[26] M. Oyaizu, Studies on products of browning reaction, Jpn. J. Nutr. Diet. 44 (6) (1986) 307–315.
[27] A.L. Waterhouse, Determination of total phenolics, Curr. Protocol Food Anal. Chem. (2002) I1.1.1–I1.1.8.
[28] S.A. Baba, S.A. Malik, Determination of total phenolic and flavonoid content, antimicrobial and antioxidant activity of a root extract of *Arisaema jacquemontii* Blume, J. Taibah Univ. Sci. 9 (4) (2015) 449–454.
[29] C.C. Chang, M.H. Yang, H.M. Wen, J.C. Chern, Estimation of total flavonoid content in propolis by two complementary colorimetric methods, J. Food Drug Anal. 10 (3) (2002).
[30] J. Zhishen, T. Mengcheng, W. Jianming, The determination of flavonoid contents in mulberry and their scavenging effects on superoxide radicals, Food Chem. 64 (4) (1999) 555–559.
[31] J. Song, H. Kong, J. Jang, Bacterial adhesion inhibition of the quaternary ammonium functionalized silica nanoparticles, Colloids Surf. B: Biointerfaces 82 (2) (2011) 651–656.
[32] A. Wojtala, M. Bonora, D. Malinska, P. Pinton, J. Duszynski, M.R. Wieckowski, Methods to monitor ROS production by fluorescence microscopy and fluorometry, Methods in Enzymology, Vol. 542 Academic Press, 2014, pp. 243–262.
[33] T. Somanathan, V.M. Krishna, V. Saravanan, R. Kumar, R. Kumar, MgO nanoparticles for effective uptake and release of doxorubicin drug: pH sensitive controlled drug release, J. Nanosci. Nanotechnol. 16 (9) (2016) 9421–9431.
[34] M. Rezaei, M. Khajenoori, B. Nematollahi, Preparation of nanocrystalline MgO by surfactant assisted precipitation method, Mater. Res. Bull. 46 (10) (2011) 1632–1637.
[35] K. Mageshwari, S.S. Mali, R. Sathyamoorthy, P.S. Patil, Template-free synthesis of MgO nanoparticles for effective photocatalytic applications, Powder Technol. 249 (2013) 456–462.
[36] P. Ouraipryvan, T. Sreethawong, S. Chavadej, Synthesis of crystalline MgO nanoparticle with mesoporous-assembled structure via a surfactant-modified sol–gel process, Mater. Lett. 63 (21) (2009) 1862–1865.
[37] A. Samariya, R.K. Singhal, S. Kumar, Y.T. Xing, M. Alzamora, S.N. Dolia, ... E.B. Saitovitch, Defect-induced reversible ferromagnetism in Fe-doped ZnO semiconductor: an electronic structure and magnetization study, Mater. Chem. Phys. 123 (2) (2010) 678–684.
[38] J.S. Kim, E. Kuk, K.N. Yu, J.H. Kim, S.J. Park, H.J. Lee, ... Y.K. Kim, Antimicrobial effects of silver nanoparticles, Nanomedicine 3 (1) (2007) 95–101.
[39] L. Bravo, Polyphenols: chemistry, dietary sources, metabolism, and nutritional significance, Nutr. Rev. 56 (11) (1998) 317–333.
[40] S. Makhluf, R. Dror, Y. Nitzan, Y. Abramovich, R. Jelinek, A. Gedanken, Microwave-assisted synthesis of nanocrystalline MgO and its use as a Bacteriocide, Adv. Funct. Mater. 15 (10) (2005) 1708–1715.
[41] B. Das, M.I. Khan, R. Jayabalan, S.K. Behera, S.I. Yun, S.K. Tripathy, A. Mishra, Understanding the antifungal mechanism of Ag@ ZnO core-shell nanocomposites against *Candida krusei*, Sci. Rep. 6 (2016).
[42] P. Stiefel, S. Schmidt-Emrich, K. Maniura-Weber, Q. Ren, Critical aspects of using bacterial cell viability assays with the fluorophores SYTO9 and propidium iodide, BMC Microbiol. 15 (1) (2015) 36.
[43] S.M. Stocks, Mechanism and use of the commercially available viability stain, BacLight, Cytometry A 61 (2) (2004) 189–195.
[44] W.O. Carter, P.K. Narayanan, J.P. Robinson, Intracellular hydrogen peroxide and superoxide anion detection in endothelial cells, J. Leukoc. Biol. 55 (2) (1994) 253–258.
[45] B. Das, M.I. Khan, R. Jayabalan, S.K. Behera, S.I. Yun, S.K. Tripathy, A. Mishra, Understanding the antifungal mechanism of Ag@ ZnO core-shell nanocomposites against *Candida krusei*, Sci. Rep. 6 (2016) 36403.
[46] S.M. Dizaj, F. Lotfipour, M. Barzegar-Jalali, M.H. Zarrintan, K. Adibkia, Antimicrobial activity of the metals and metal oxide nanoparticles, Mater. Sci. Eng. C 44 (2014) 278–284.